# Research Article



Received: 31 October 2022

Revised: 12 February 2023

Accepted article published: 26 February 2023

Published online in Wiley Online Library: 10 March 2023

(wileyonlinelibrary.com) DOI 10.1002/jctb.7345

# Catalytic effects of molybdate and chromate-molybdate films deposited on platinum for efficient hydrogen evolution

Oscar Diaz-Morales,<sup>a</sup> • Aleksandra Lindberg,<sup>b\*</sup> • Vera Smulders,<sup>c</sup> • Athira Anil,<sup>d</sup> Nina Simic,<sup>e</sup> Mats Wildlock,<sup>e</sup> Germán Salazar Alvarez,<sup>d</sup> • Guido Mul,<sup>c</sup> • Bastian Mei<sup>c,f</sup> • and Ann Cornell<sup>b\*</sup> •



#### **Abstract**

BACKGROUND: Sodium chlorate (NaClO<sub>3</sub>) is extensively used in the paper industry, but its production uses strictly regulated highly toxic  $Na_2Cr_2O_7$  to reach high hydrogen evolution reaction (HER) Faradaic efficiencies. It is therefore important to find alternatives either to replace  $Na_2Cr_2O_7$  or reduce its concentration.

RESULTS: The  $Na_2Cr_2O_7$  concentration can be significantly reduced by using  $Na_2MoO_4$  as an electrolyte co-additive.  $Na_2MoO_4$  in the millimolar range shifts the platinum cathode potential to less negative values due to an activating effect of cathodically deposited Mo species. It also acts as a stabilizer of the electrodeposited chromium hydroxide but has a minor effect on the HER Faradaic efficiency. X-ray photoelectron spectroscopy (XPS) results show cathodic deposition of molybdenum of different oxidation states, depending on deposition conditions. Once  $Na_2Cr_2O_7$  was present, molybdenum was not detected by XPS, as it is likely that only trace levels were deposited. Using electrochemical measurements and mass spectrometry we quantitatively monitored  $Na_2$  and  $Na_2$  production rates. The results indicate that 3  $\mu$ mol  $L^{-1}$   $Na_2Cr_2O_7$  (contrary to current industrial 10–30 mmol  $L^{-1}$ ) is sufficient to enhance the HER Faradaic efficiency on platinum by 15%, and by co-adding 10 mmol  $L^{-1}$   $Na_2MoO_4$  the cathode is activated while avoiding detrimental  $Na_2$  generation from chemical and electrochemical reactions. Higher concentrations of  $Na_2MoO_4$  led to increased oxygen production.

CONCLUSION: Careful tuning of the molybdate concentration can enhance performance of the chlorate process using chromate in the micromolar range. These insights could be also exploited in the efficient hydrogen generation by photocatalytic water splitting and in the remediation of industrial wastewater.

© 2023 The Authors. Journal of Chemical Technology and Biotechnology published by John Wiley & Sons Ltd on behalf of Society of Chemical Industry (SCI).

Supporting information may be found in the online version of this article.

**Keywords:** hydrogen evolution reaction; chlorate process; molybdenum; chromate

## INTRODUCTION

Sodium chlorate (NaClO<sub>3</sub>) is one of the largest (by volume) electrochemically produced materials, with a yearly production capacity of approximately 4 million tons. <sup>1</sup> It is the precursor of chlorine dioxide (ClO<sub>2</sub>), which is extensively used in the paper industry to bleach pulp feedstock. This bleaching technology, i.e. elemental chlorine-free (ECF) bleaching, is regarded as the best available technique. No other bleaching technology provides the same brightness while retaining the strength of the pulp, good economy and very low environmental impact. <sup>2</sup>

The chlorate process is an electrochemical process carried out in undivided electrochemical cells. It consists of a complex series of electrochemical and chemical reactions that convert chloride ions into chlorate, with hypochlorous acid and hypochlorite anions as intermediates. Concomitantly, hydrogen evolution (2H<sub>2</sub>O + 2e $^ \rightarrow$  H<sub>2</sub> + 2OH $^-$ ) takes place on the cathodes.<sup>3</sup>

- \* Correspondence to: Aleksandra Lindberg or Ann Cornell, Applied Electrochemistry, School of Engineering Sciences in Chemistry, Biotechnology and Health, KTH Royal Institute of Technology, SE 100-44, Stockholm, Sweden. E-mail: stojano@kth.se (Lindberg); E-mail: amco@kth.se (Cornell)
- a TNO/Holst Centre, Eindhoven, The Netherlands
- b Applied Electrochemistry, School of Engineering Sciences in Chemistry, Biotechnology and Health, KTH Royal Institute of Technology, Stockholm, Sweden
- c PhotoCatalytic Synthesis Group, MESA+ Institute for Nanotechnology, Faculty of Science and Technology, University of Twente, Enschede, The Netherlands
- d Department of Materials Science and Engineering, Uppsala University, Uppsala, Sweden
- e Nouryon, Bohus, Sweden
- f Industrial Chemistry, Faculty of Chemistry and Biochemistry, Ruhr University Bochum, Bochum, Germany

SCI.
where science
meets business

Since the process is performed in undivided cells, electroreduction of hypochlorite and chlorate anions can occur. These unwanted reactions reduce the energy efficiency of the process and are conventionally minimized by adding 3-6 g dm<sup>-3</sup> Na<sub>2</sub>Cr<sub>2</sub>O<sub>7</sub> to the electrolyte. <sup>4</sup> The Cr<sup>VI</sup> additive gets reduced during electrolysis and forms a poorly electrically conductive film of hydrous chromium(III) oxide/hydroxide (here denoted as  $Cr(OH)_3 \times nH_2O$ ) on the cathode, which hinders the transport of hypochlorite and chlorate anions to the electrode surface, thus preventing their electroreduction.  $Cr(OH)_3 \times nH_2O$  still allows water to reach the cathode surface so the hydrogen evolution reaction (HER) can proceed in the presence of the film.<sup>4,5</sup> An alternative mechanism explaining the selectivity of the  $Cr(OH)_3 \times nH_2O$  film has been suggested to be electrocatalytic, where Density Functional Theory (DFT) calculations show that the active site for hypochlorite reduction becomes blocked in the course of reduction by irreversible hydroxylation of the transition metal site during the reaction.<sup>6</sup>

 $Na_2Cr_2O_7$  is pivotal in producing  $NaClO_3$  efficiently; without this additive it is not possible to produce chlorate with the currently available technologies. Unfortunately, all  $Cr^{VI}$  compounds are environmentally harmful and have proven to be carcinogenic, mutagenic and reprotoxic to humans, and therefore included in the REACH annex XIV list of the European Union (EU). To Thus, since 2017, a special authorization is required to use  $Cr^{VI}$  compounds within the EU. Despite many research efforts devoted to finding less harmful alternatives to the  $Na_2Cr_2O_7$  additive for the chlorate process, Or Cround to the complex role of this additive as well as the harsh operating conditions (i.e. highly oxidizing electrolyte and high temperature).

Molybdate (MoO<sub>4</sub><sup>2-</sup>) has been investigated as a full or partial replacement to Na<sub>2</sub>Cr<sub>2</sub>O<sub>7</sub> addition. Molybdate addition influences the chlorate process in several ways: (i) it activates the HER on cathodes of titanium, <sup>18,19</sup> molybdenum<sup>19</sup> and steel; <sup>17</sup> (ii) it enhances the current efficiency towards HER on steel/iron and titanium; 11,20 and (iii) it increases the rate of unwanted oxygen formation, in particular at high molybdate concentrations. 17,18 Note that all these studies were made on the industrially relevant electrode materials iron/steel and titanium, which undergo reactions such as oxidation and hydride formation in the chlorate electrolyte. Steel corrodes when not under cathodic protection, and the different types of corrosion products influence the chemical and electrochemical reactions.<sup>12</sup> Even under cathodic polarization, corrosion products are not completely reduced under conditions for hydrogen evolution at non-noble materials such as steel and titanium.<sup>21</sup> On a hydrogen-evolving titanium cathode, a layer of titanium hydride is formed, changing the electrochemical properties of the electrode. This continuous change of properties of steel and titanium cathodes is also seen in full-scale operations.<sup>22</sup> Thus, to pinpoint and further understand the role of the molybdate additive on HER electrocatalysis, we have conducted a study using platinum cathodes, which are regarded as being more inert and highly active for HER. This approach is supported by two recent reports: one study showing that electrodeposited molybdenum on single-crystal platinum electrodes activates the HER in alkaline solution by influencing the binding strength of the adsorbed hydroxide intermediate;<sup>23</sup> and another, on glycerol oxidation and HER, showing a synergistic electrocatalytic effect between platinum and molybdenum oxide.<sup>24</sup>

Chromium-based and molybdenum-based oxides are not only relevant for the chlorate process, but are also used for efficient

hydrogen generation in photocatalytic water splitting. <sup>25-27</sup> The selective, permeable films there hinder the recombination of  $H_2$  and  $O_2$  back to  $H_2O$ . <sup>28</sup> The selective permeability has been exploited to drive the photocatalytic degradation of harmful wastes (e.g. sulfide). <sup>29</sup> Addition of Pt to chromium-formed films is beneficial as an effective cocatalyst for photocatalytic water splitting. <sup>30</sup> Therefore, understanding the role of  $MoO_xH_y$  films and of their synergy with  $CrO_xH_y$  on catalytic reactions has a wide range of implications for sustainable fuel generation and the remediation of wastewater.

Here, the synergetic effect of Cr–Mo on the efficiency for hydrogen generation in NaClO-containing electrolytes has been studied using platinum cathodes. Concentration limits of Na<sub>2</sub>MoO<sub>4</sub> were explored, aiming to run the chlorate process at low Na<sub>2</sub>Cr<sub>2</sub>O<sub>7</sub> concentrations. Formed films were characterized by scanning electron microscopy (SEM) and X-ray photoelectron spectroscopy (XPS), and their influence on activity and selectivity towards HER, oxygen formation and hypochlorite reduction was investigated. Furthermore, it was found that *in situ* formed Cr–Mo mixed metal oxide films are chemically stable, providing essential benefits for cathode corrosion protection during process shutdown.

## **EXPERIMENTAL**

#### Surface characterization of the formed films

The Pt used as working electrode (rotating disc or foil) was mechanically polished to a mirror finish with alumina of decreasing grain size of 5, 0.3 and 0.05  $\mu mol~L^{-1}$ , prior to each experiment. Afterwards, it was thoroughly rinsed and sonicated for 10 min with ultrapure water (resistivity > 18.2 M $\Omega$  cm) to remove polishing residues. After mechanical polishing, the Pt electrode was electrochemically cleaned/activated by performing cyclic voltammetry between 0 and 0.75 V versus Ag/AgCl at 100 mV s $^{-1}$  in a 0.1 mol L $^{-1}$  NaOH (>99% Sigma Aldrich, Stockholm, Sweden).

For surface characterization experiments, cathodic depositions were formed on Pt foil polarized in 0.1 mol L $^{-1}$  NaOH, at -0.8 V versus Ag/AgCl for 5 min, using a Pt wire as a counter electrode and a Hg/HgO as a reference, while purging the electrolyte by N $_2$ . After 5 min the samples were removed from the electrolyte without interrupting polarization. Different concentrations of additive in the form of Na $_2$ MoO $_4 \times 2H_2O$  (used as received from Sigma Aldrich, Stockholm, Sweden) were added and samples are named accordingly; for example, the sample with 10 mmol L $^{-1}$  Mo salt formed at 22 °C (which was the room temperature when preparing these samples, noted as RT) is 10Mo-22 (see also Table 1). Finally, the samples were rinsed with water, ethanol and acetone.

Scanning electron microscopy (SEM) images were acquired using a Hitachi S-4800 instrument at 1 kV accelerating voltage,

Table 1.         Sample naming for characterization by SEM and XPS			
Sample	Name		
(A) 10 mmol L <sup>-1</sup> Mo, 22 °C (B) 80 mmol L <sup>-1</sup> Mo, 22 °C (C) 10 mmol L <sup>-1</sup> Mo, 80 °C (D) 80 mmol L <sup>-1</sup> Mo, 80 °C (E) 10 mmol L <sup>-1</sup> Mo, 3 μmol L <sup>-1</sup> Cr, 22 °C (F) 80 mmol L <sup>-1</sup> Mo, 3 μmol L <sup>-1</sup> Cr, 22 °C	10Mo-22 80Mo-22 10Mo-80 80Mo-80 10Mo-3Cr-22 80Mo-3Cr-22		

10974660, 2023. 5, Downloaded from https://onlinelibrary.wiley.com/doi/10.1002/jctb.7345 by Cochrane Netherlands, Wiley Online Library on [1890] 2023]. See the Terms and Conditions (https://onlinelibrary.wiley.com/terms-and-conditions) on Wiley Online Library for rules of use; OA articles are governed by the

to avoid damaging samples. A Quantera II scanning XPS microprobe instrument having monochromatic Al K $\alpha$  radiation with a total power of 50 W was used for the XPS measurements. The beam spot size was 100 µm<sup>2</sup>, and the base pressure of the main chamber was  $7 \times 10^{-7}$  bar. Survey scans were taken using five different sample regions to check the repeatability and uniformity of the samples. Survey scans were recorded from 1040 to 0 eV with a pass energy of 224 eV. In addition, high-resolution core shell elemental electronic spectra were taken using 55 eV pass energy and 0.05 eV resolution. CASA XPS<sup>31</sup> was used for further XPS analysis and deconvolution of peaks. The Mo individual peak area was determined using integration, having Shirley as the background function.

#### Catalytic effect of Mo on HER

The experiments were performed with a platinum rotating disc electrode (RDE) of 5 mm diameter from PINE Research (model WaveVortex 10 RDE). Polarization curves were recorded galvanostatically from high to low current density using a BioLogic model VSP (Figs 3 and 4) or a PAR 273A potentiostat (Figs 2 and 5). To correct for the IR drop a built-in high-frequency impedance method (85% correction) was used with Biologic, whereas a current interrupt technique (100% correction) was used with the PAR potentiostat. In the latter, for each current density level the electrode was polarized for 15 s and then the current was interrupted repeatedly. The potential decay was measured for 500 μs at 1 MHz data sampling and recorded potential data were fitted using a third-order polynomial expression to establish the IRcorrected potential values. 32,33

A three-electrode system was employed, in which a Pt RDE was the working electrode, a Pt wire was the counter electrode and Ag/AgCl (3 mol  $L^{-1}$  KCl) or Hg/HgO (1 mol  $L^{-1}$  NaOH) was the reference electrode. When the electrolyte did not contain chloride ions a single compartment cell was used. For the polarization curve experiments using chloride in the electrolyte, the CE was placed in a compartment separated from the WE by a frit to inhibit the reaction products at the CE (hypochlorite) to reach the WE. The potentials reported in this work are all referred to an Ag/AgCl reference electrode, which were calculated according to Egn (1):

$$E_{Ag/AgCI} = E_{Hg/HgO} - 0.065V \tag{1}$$

Electrode transfer for experiments with ex situ formed films were performed by first pre-polarizing the electrodes in hypochlorite-free solutions containing the desired additives for 5 min at -0.8 V versus Ag/AgCl and removed without interrupting polarization. The electrodes were then rinsed with water and transferred to a clean electrolyte containing 0.1 mol  $L^{-1}$  NaOH, 2 mol L<sup>-1</sup> NaCl and 80 mmol L<sup>-1</sup> NaClO or only 0.1 mol L<sup>-1</sup> NaOH. Polarization curves were recorded from high to low current density, with constant N<sub>2</sub> flow.

### Effect of Mo and Cr in situ electrolyte additions on the Faradaic efficiency for hydrogen and oxygen evolution

These measurements were done with a residual gas analyzer (RGA) operating with a triple-filter quadrupole mass spectrometer from Hiden (model HPR-20). This instrument is equipped with a heated quartz capillary that allows connecting the headspace of the electrochemical cell (at room pressure, ~760 torr) with the mass spectrometer chamber ( $\sim 10^{-6}$  torr).

A gas-tight, two-electrode electrochemical cell was used for the mass spectrometry (MS) experiments, as previously reported by our group. 13,14,16,34 A Pt foil was used as working electrode and a dimensionally stable anode (Ti<sub>0.7</sub>Ru<sub>0.3</sub>) as a counter electrode. Both working and counter electrodes had ~0.5 cm<sup>2</sup> of geometric surface area. Measurements were performed during galvanostatic electrolysis at 300 mA cm<sup>-2</sup><sub>geo</sub>, with flow of Ar as a carrier gas of 75 mL min<sup>-1</sup>. In addition, to study oxygen formation from homogeneous reactions in the bulk electrolyte, MS measurements were made without the presence of any electrodes in the cell.

The electrolyte contained 2 mol L<sup>-1</sup> NaCl and an initially 80 mmol L<sup>-1</sup> NaClO (both chemicals were purchased from VWR International, Spånga, Sweden and were used as received). Experiments were performed at 80 °C with the electrolyte adjusted and kept at pH 6.5 with an automatic titrator Metrohm 907 Titrando titrator equipped with a Unitrode and Pt 1000 combined pH and temperature sensor. The electrolyte pH was kept constant by adding either 6 mol L<sup>-1</sup> HCl or 1 mol L<sup>-1</sup> NaOH.

NaClO concentration was monitored as a function of time by analyzing liquid samples by ex situ ultraviolet-visible spectroscopy, following a previously reported procedure. 15,32

#### RESULTS AND DISCUSSION

#### Surface characterization of formed films

The formed films indicated in Table 1 were analyzed by SEM and energy-dispersive X-ray analysis (EDX). No clear depositions could be seen on the platinum surface (Supporting Information Fig. S1). Probably, the formed films were of the order of nanometer thickness and therefore too thin for EDX measurements, which only recorded Pt peaks (Supporting Information Fig. S2). In addition, X-ray emission lines of Pt and Mo are very close in energy, and the Pt peak responses possibly overlaps the Mo peaks. 35

However, the more surface-sensitive XPS identified elements present in the samples as well as oxidation states of Mo (Supporting Information Fig. S3). Molybdenum has oxidation states ranging from +2 to +6. Considering the importance of Mo oxidation state for different applications such as gas sensors, energy storage (desired Mo<sup>VI</sup>) or as anodic material for the solid oxide fuel cells (desired Mo<sup>IV</sup>), different techniques to obtain certain Mo oxidation states have been employed.<sup>36-38</sup> Here, we deposited Mo layers from aqueous solutions and used XPS to evaluate the oxidation state of the electrodeposited Mo films as a function of the plating conditions (i.e. temperature and molybdate concentration). The deconvoluted core-level electronic spectra of Mo and Pt are shown in Fig. 1 and Supporting Information Fig. S4, respectively. The Pt core-level spectra show two well-resolved peaks corresponding to the Pt 4f7/2 and Pt 4f5/2 asymmetric representing metallic Pt. In the case of Mo, the prominent Mo peak and its intensity vary in all four samples, suggesting that each sample is unique regarding the different oxidation states. Compared to the electrolyte solution of MoO<sub>3</sub>, where the Mo oxidation state is +6, partial reduction to lower oxidation states is observed in all the four samples. Peak positions and oxidation state percentages are shown in Table 2, and the peak positions go well with earlier reported values. 39,40 Films deposited at higher temperatures show higher percentages of higher oxidation states (+6 and + 5) compared to the films deposited at room temperature.

In all samples Ag was recorded, and by recording pure Pt foil used for samples deposition the presence of Ag was confirmed, indicating that the Ag response comes from the substrate itself.

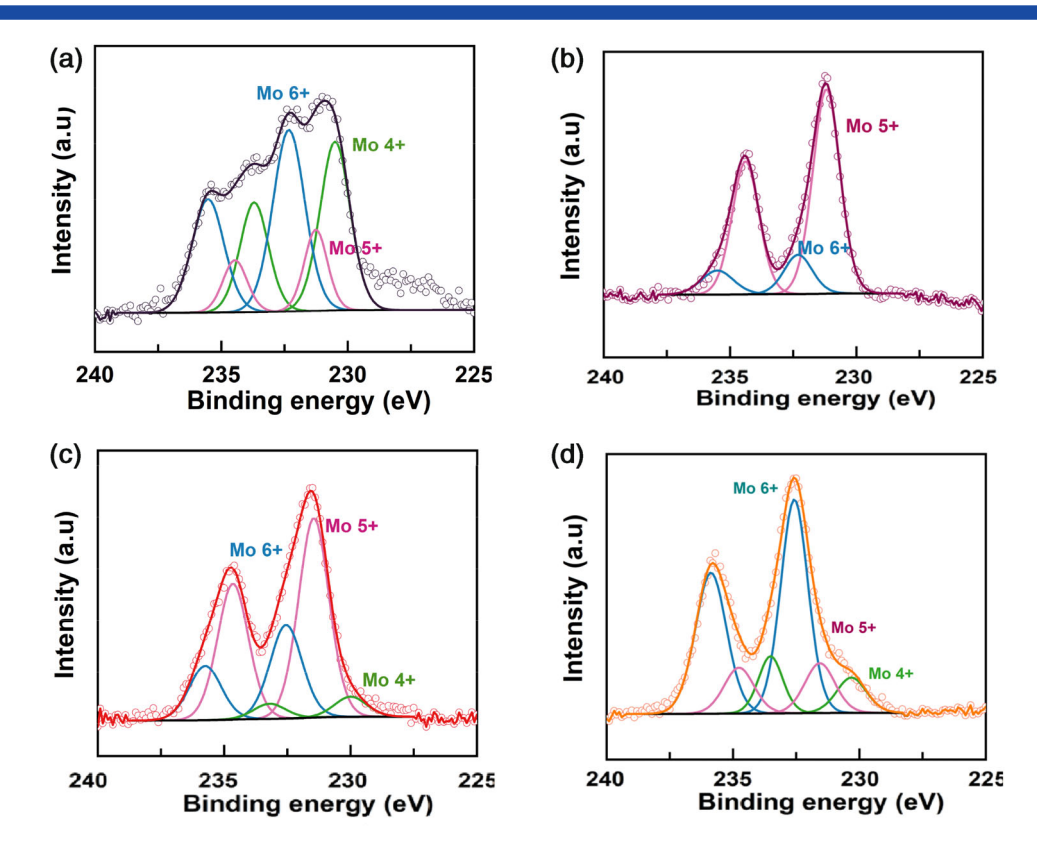


**Figure 1.** XPS spectra of films synthesized on Pt foil polarized on -0.8 V *versus* Ag/AgCl for 5 min and removed while polarizing, in 0.1 mol L<sup>-1</sup> NaOH working electrolyte with Mo addition up to concentrations of (a) 10 mmol L<sup>-1</sup> Mo, 22 °C; (b) 80 mmol L<sup>-1</sup> Mo, 22 °C; (c) 10 mmol L<sup>-1</sup> Mo, 80 °C; and (d) 80 mmol L<sup>-1</sup> Mo, 80 °C.

The film deposited in an electrolyte containing 3  $\mu$ mol L<sup>-1</sup> Cr and 10 (or 80) mmol L<sup>-1</sup> Mo displayed response characteristics only for Cr, with no signs of any Mo deposited (Supporting Information Fig. S5). An earlier study employing XPS found that Mo did not deposit from solutions containing Mo and phosphate ions.<sup>19</sup> It was discussed that there could be a few different reasons for that, such as the formation of some interfering metal phosphate or competitive adsorption of molybdate and phosphate. In the case of Mo–Cr films, a similar phenomenon could be operating. Another possibility is that a Cr-hydroxide film is formed, which hinders molybdate reduction and, therefore, subsequent Mo deposition.<sup>18</sup>

Interestingly, it was found that more Mo is electrodeposited from pH-neutral solutions compared to deposition at higher pH.<sup>19</sup> Deposits formed in alkaline solutions showed two main peaks, located at 232.6 eV and 230.4 eV, assigned to MoO<sub>3</sub> and MoO<sub>2</sub>. Reports indicate that formed films were either very thin or formed locally, as the signal from substrate (in the reported

**Table 2.** Mo oxidation states determined by XPS and its percentage in each sample Sample/Mo oxidation state +4 +5 +6 39.5 15 10Mo-22 45.5 80Mo-22 85.5 14.5 10Mo-80 63.6 29.4 80Mo-80 15.7 18.5 65.8 10Mo-3Cr-22 80Mo-3Cr-22

case, Ti) was recorded on these samples. Here, we agree with previous reported values for positions of the peaks for Mo +4 and +6 (Table 3). <sup>19</sup> We also record Mo in +5 state, mainly in the samples 80Mo-22 and 10Mo-80.

# Catalytic effect of Mo on HER

IR-corrected polarization curves were recorded to analyze the effect of Mo addition on HER on a Pt electrode (Fig. 2). The study was performed under alkaline conditions as it represents the electrolyte close to a cathode where hydroxide ions formed during HER cause a locally increased pH. The cathode potential at the industrially relevant current density 300 mA cm $^{-2}$  shifted 126 mV to a less negative potential when Mo was present in the electrolyte at 10 mmol L $^{-1}$ , compared to Mo-free electrolyte (Fig. 2(a)). Further increase in the molybdate concentration to 80 mmol L $^{-1}$  deactivated the electrode; compared to the 10 mmol L $^{-1}$  case, it shifted 50 mV to a more negative potential. This was likely due to a thick layer being formed by the higher Mo concentration and is in line with previous observations,  $^{19}$  where it was realized that the concentration of

<b>Table 3.</b> Peak positions (binding energy) for different Mo oxidation states				
Sample ID	Mo <sup>+4</sup> BE (eV)	Mo <sup>+5</sup> BE (eV)	Mo <sup>+6</sup> BE (eV)	
10Mo-22	230.3	231.2	232.4	
80Mo-22	_	231.2	232.4	
10Mo-80	230.1	231.3	232.5	
80Mo-80	230.3	231.5	232.6	



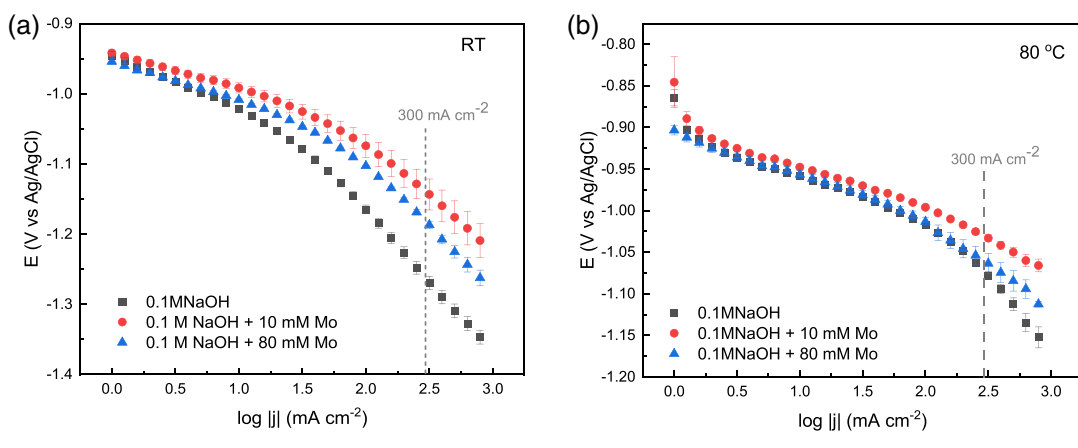


Figure 2. IR-corrected polarization curves recorded in 0.1 mol L<sup>-1</sup> NaOH with in situ addition of marked Mo concentration, at 2500 rpm, with constant purging by N<sub>2</sub> at (a) RT and (b) 80 °C. The cathode was pre-polarized at -0.8 V versus Ag/AgCl for 5 min before measuring the polarization curve from high to low current density. The grey dashed line indicates the current density typically used industrially (300 mA cm<sup>-2</sup>).

4 mmol L<sup>-1</sup> Mo addition had a stronger activating effect than 100 mmol L<sup>-1</sup> Mo, regardless of the substrate material. The same trend was observed also at higher temperature (80 °C; Fig. 2(b)).

Polarization curves recorded at RT reveal two regions. Without any Mo additive the Tafel slope was around -190 mV dec<sup>-1</sup> in the higher current density region. Molybdate addition lowered the Tafel slopes: with addition of 80 mmol L<sup>-1</sup> Mo it was -175 mV dec<sup>-1</sup> and with 10 mmol L<sup>-1</sup> Mo addition it amounted to -150 mV dec<sup>-1</sup>. A similar trend was recorded in the lower current density region: without Mo addition the Tafel slope was -73 mV dec<sup>-1</sup>; with 80 mmol L<sup>-1</sup> Mo it was -63 mV dec<sup>-1</sup>; and with 10 mmol  $L^{-1}$  Mo addition it was -57 mV  $dec^{-1}$ . A Tafel slope of 125 mV  $dec^{-1}$  has been reported for HER on Pt in 0.5 mol  $L^{-1}$ NaOH. 41 However, values in the range 100–130 mV dec<sup>-1,42</sup> or even lower, were found with Pt-based and modified catalysts. 43,44

The differences can be assigned to different pH values of the electrolytes in the studies, and to the potential dependence of the Tafel slope.45

Another difference among the samples is the difference in oxidation state of Mo, directly after deposition (Table 2). The highest activity towards HER was recorded on the sample where the +6 oxidation state dominates, i.e. with addition of 10 mmol  $L^{-1}$  Mo.

Pt catalysts typically have lower activity for HER in alkaline media compared to acidic, due to the sluggish water dissociation step. Therefore, some elements such as Mo may be added to Pt to provide active sites for the sluggish step and significantly improve Pt activity in alkaline media. When combining molybdenum oxide sheets with Pt nanoparticles, the activity towards HER compared to pure Pt was improved.<sup>24</sup> However, it is likely that Pt was the material providing active sites for the HER, as a pure Mo electrode showed poorer HER performance than pure Pt. Recently it was shown, by combining DFT calculations and experimental work, that once Mo is added to Pt the energy of hydroxide adsorption is high, indicating that the rate-determining step in HER is actually hydroxide desorption.<sup>23</sup> The Pt-Mo catalyst was found to be bifunctional for HER, involving both adsorbed hydrogen and adsorbed hydroxide.

The polarization curves measured on the Pt RDE at 2500 rpm in 2 mol L<sup>-1</sup> NaCl (Fig. 3) illustrate the system with three different concentrations of Na<sub>2</sub>CrO<sub>7</sub>. The black open squares curve, acquired in the absence of NaClO, shows a monotonic increase in potential at high current densities, as expected for the HER.

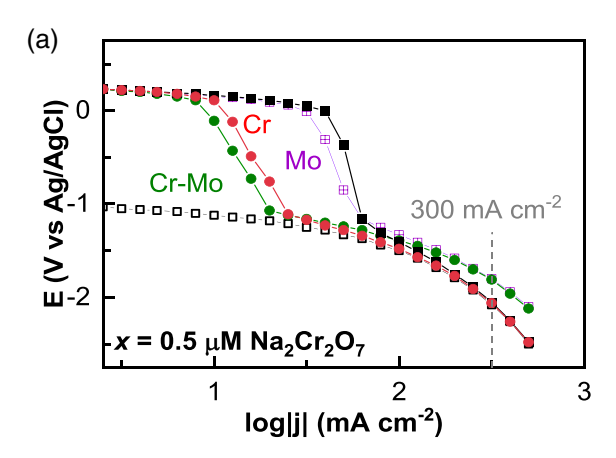
The black filled squares curve was acquired in the presence of NaClO (without chromate and molybdate additives). This curve shows a limiting current between 0 and - 1 V versus Ag/AgCl, which relates to hypochlorite reduction, whereas HER is the dominating reaction at potentials negative to -1 V versus Aq/AqCl.

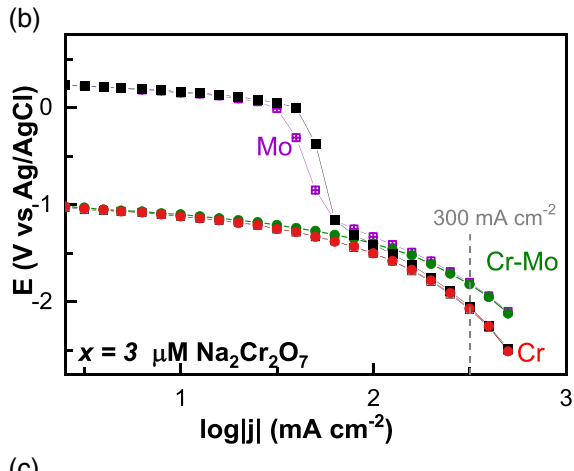
Upon adding 0.5 μmol L<sup>-1</sup> Na<sub>2</sub>CrO<sub>7</sub> to the electrolyte (red curve in Fig. 3(a)), the limiting current corresponding to hypochlorite electroreduction shifts to lower current densities, indicating partial inhibition of the reaction. At chromate concentrations higher than 3  $\mu$ mol L<sup>-1</sup> in the electrolyte (see red curves in Figs. 3(b, c)) full inhibition of the hypochlorite electroreduction occurred, in agreement with previous reports. 11 With an increase in chromate concentration the thickness of the chromate film formed increases, leading to an increase in the performance.46 However, here we see that there is a critical concentration of Cr needed for suppression of hypochlorite reduction. It is also important to note that the polarization curves acquired with CrVI in solution overlap with the curve obtained without hypochlorite at potentials negative to -1 V versus Aq/AqCl, indicating that HER is not much affected by the presence of the Cr film.

The molybdate additive affects both the hypochlorite electroreduction and the HER, as seen in the purple curve in Fig. 3. The limiting current corresponding to hypochlorite electroreduction shifts to lower current densities when 10 mmol L<sup>-1</sup> Na<sub>2</sub>MoO<sub>4</sub> is added to the electrolyte, depicting a small retarding effect of the MoO<sub>x</sub>H<sub>v</sub> film on the hypochlorite electroreduction. An increase in cathodic current efficiency at small chromate concentrations in the presence of molybdate was recently reported.<sup>18</sup> The cathode potential shifts to less negative potentials in the presence of the molybdate additive: when the  $Cr^{VI}$  concentration amounts to 13.5  $\mu$ mol  $L^{-1}$ , the cathode potential shifts 260 mV to less negative values at 300 mA cm<sup>-2</sup> compared to the values obtained in molybdate-free electrolytes. Also, the inhibiting effect of molybdate on the hypochlorite reduction could be further enhanced by adding low amounts of chromate to the electrolyte (see polarization curves in green in Fig. 3), while the activation towards hydrogen evolution remains as in the case of only molybdate present. The inhibiting and activating effects of the molybdate additive have been previously reported. 11,17,18,47 However, those studies used higher molybdate concentrations (>40 mmol L<sup>-1</sup> Na<sub>2</sub>MoO<sub>4</sub>), leading to undesired enhancement in O<sub>2</sub> generation. Here, we show hypochlorite electroreduction hindrance with chromate (3  $\mu$ mol L<sup>-1</sup>) and molybdate (10 mmol L<sup>-1</sup>) 10974660, 2023, 5, Downloaded from https://onlinelibrary.wiley.com/doi/10.1002/jctb.7345 by Cochrane Netherlands, Wiley Online Library on [18/09/2023]. See the Terms and Conditions (https://onlinelibrary.wiley.com/terms-and-conditions) on Wiley Online Library for rules of use; OA articles are governed by the

10974660, 2023, 5, Downloaded from https://onlinelibrary.wiley.com/doi/10.1002/jctb.7345 by Cochrane Netherlands, Wiley Online Library on [18/09/2023]. See the Terms

) on Wiley Online Library for rules of use; OA articles are governed by the applicable Creative Commons License





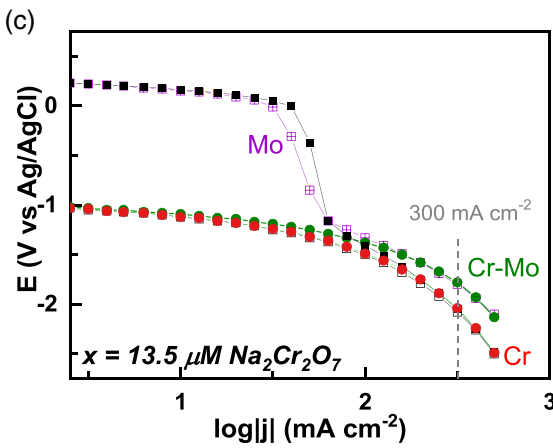


Figure 3. IR-corrected polarization curve for hydrogen evolution reaction (HER) in NaClO<sup>-</sup>-containing electrolyte, as a function of the concentration of Na<sub>2</sub>Cr<sub>2</sub>O<sub>7</sub> additive (x) in the absence and presence of molybdate co-additive: (a)  $x = 0.5 \mu$ mol L<sup>-1</sup>; (b)  $x = 3 \mu$ mol L<sup>-1</sup>; (c)  $x = 13.5 \mu$ mol L<sup>-1</sup>. Measurements were made at 2500 rpm at RT. Pre-polarization at  $-0.8 \text{ V } \text{ versus } \text{ Ag/AgCl } \text{ for } 5 \text{ min before measuring the polarization curve from high to low current density, with constant purging by N<sub>2</sub>. The grey dashed line indicates the current density typically used to run the industrial chlorate process (300 mA cm<sup>-2</sup>).$ 

in solution, having less negative cathode potential compared to the reaction performed in additive-free electrolyte. Note that although the XPS results indicate that Mo deposition is hindered by the

presence of Cr, there is still an activation of HER in Fig. 3 in a Crcontaining electrolyte. To better understand this, the HER was investigated on *ex situ* formed films.

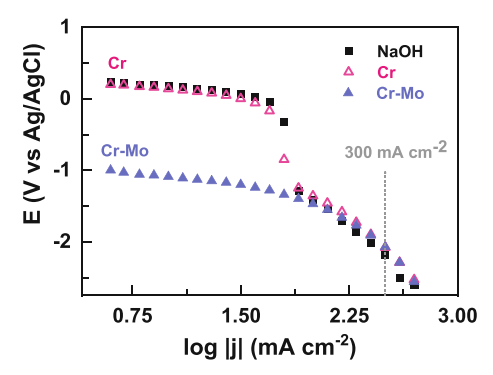


Figure 4. IR-corrected polarization curves at 2500 rpm at RT, acquired with a cathode ex situ coated with oxide films in 0.1 mol L<sup>-1</sup> NaOH, 2 mol L<sup>-1</sup> NaCl and 80 mmol L<sup>-1</sup> hypochlorite. Ex situ formed films were deposited at -0.8 V versus Ag/AgCl for 5 min in solutions (without NaClO), with either  $Na_2Cr_2O_7$  solution (13.5  $\mu$ mol L<sup>-1</sup>), a mixture of  $Na_2Cr_2O_7$ (13.5  $\mu$ mol L<sup>-1</sup>) and Na<sub>2</sub>MoO<sub>4</sub> (80 mmol L<sup>-1</sup>) or without any additives (NaOH marks).

#### Ex situ formed catalytic cathodic films

The apparent activation of HER by Mo may be explained by either a catalytically active Mo oxide species or by continuous reduction of dissolved molybdate. 17,19 To determine the source of the activating effect, polarization curves for hydrogen evolution on ex situ coated cathodes were obtained in hypochlorite-containing electrolyte (Fig. 4). The electrodes with ex situ formed films were removed from the depositing electrolyte while still polarized. Afterwards, the electrode was rinsed and transferred to the measuring electrolyte (NaOH 0.1 mol L<sup>-1</sup> + NaCl 2 mol L<sup>-1</sup> + NaClO 80 mmol L<sup>-1</sup>). Insertion in the measuring electrolyte was done under open circuit conditions. As revealed by the pink curve in Fig. 4, the ex situ formed films, deposited in chromate-containing electrolyte (13.5  $\mu$ mol L<sup>-1</sup> Na<sub>2</sub>Cr<sub>2</sub>O<sub>7</sub>) only, are not stable. In fact the inhibiting effect on hypochlorite reduction disappear upon transfer (compare red curves in Figs 3(c) and 4). Conversely, the film deposited in a mixture of chromate and molybdate maintains the inhibiting effect on hypochlorite reduction after transfer. This clearly shows that molybdenum enhances the stability of the film in an alkaline environment under open circuit conditions, enhancing the corrosion protection greatly. Furthermore, for ex situ coatings formed by Mo addition, the polarization curves resemble the trend observed for in situ formed films (Fig. 2); that is, 10 mmol L<sup>-1</sup> Mo improves the activity for HER most efficiently, indicating a true activation of HER by the formed films rather than a simultaneous continuous Mo reduction shifting the potential (Fig. 5).

## Effect of Mo and Cr electrolyte in situ additions on the Faradaic efficiency for hydrogen and oxygen evolution

Faradaic efficiencies of hydrogen and oxygen evolution were measured under experimental conditions approaching the industrial ones, by increasing the temperature to 80 °C and maintaining the bulk electrolyte at pH 6.5. To assess the role of additives, galvanostatic electrolysis with simultaneous MS measurements were performed. The effect of chromate and molybdate additives on the Faradaic efficiency towards hydrogen evolution, measured after 30 min of galvanostatic electrolysis, is depicted in Fig. 6 (the hypochlorite concentration in the electrolyte reached a constant value of  $\sim$ 30 mmol L<sup>-1</sup>, as shown in Supporting Information Fig. S6). The Faradaic efficiency towards hydrogen evolution is calculated as the ratio of the volumetric flow of hydrogen after

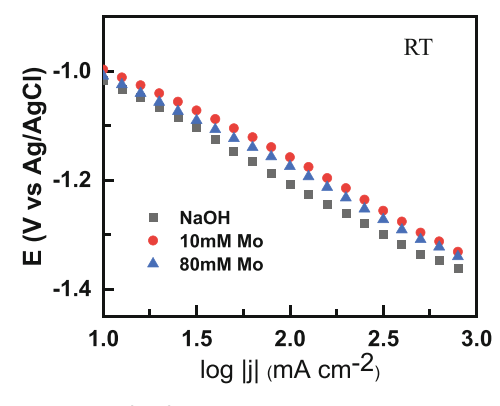


Figure 5. IR-corrected polarization curves at 2500 rpm at RT, acquired with a cathode ex situ coated with oxide films in 0.1 mol L<sup>-1</sup> NaOH. Ex situ formed films were deposited at -0.8 V versus Ag/AgCl for 5 min in solutions without any additives (NaOH marks) or with Mo additions up to concentrations of 10 and 80 mmol  $L^{-1}$ .

30 min of electrolysis with respect to the expected flow of hydrogen for the applied current (22.65  $\mu$ L s<sup>-1</sup>). The volumetric flow of H<sub>2</sub> as a function of time is shown in Supporting Information Fig. S7.

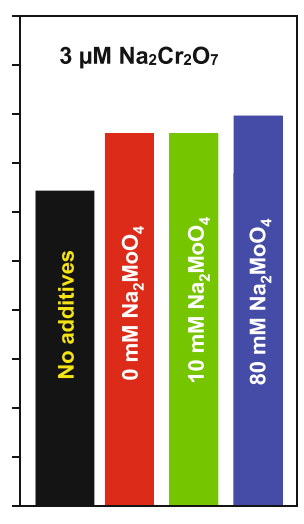
The results show that the Faradaic efficiency to hydrogen is only  $\sim$ 65% in the absence of chromate and molybdate additives. This observation agrees well with the polarization curve in Fig. 3, where it is clearly shown that, in the absence of chromate or molybdate, hypochlorite anions can be electrochemically reduced on the Pt working electrode. The MS results in Fig. 6 also indicate that  $0.5 \mu mol L^{-1}$  of chromate additive does not significantly affect the efficiency of hydrogen production on Pt in NaClO<sup>-</sup>-containing electrolyte. With these low concentrations of chromate in solution, adding 80 mmol L<sup>-1</sup> of molybdate induces a small enhancement, in line with previous reports. 11

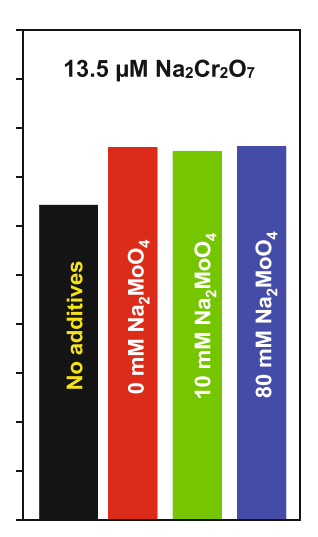
By increasing the concentration of chromate in solution (i.e. 3 and 13.5  $\mu$ mol L<sup>-1</sup>), the efficiency towards hydrogen generation enhances to >75%, as one would expect due to the inhibiting effect of chromate. 10,12,20,46,48-51 Note that this is far below the Faradaic efficiency obtained industrially of close to 100%, then with electrolyte levels of  $\sim 3-6$  g L<sup>-1</sup> Na<sub>2</sub>Cr<sub>2</sub>O<sub>7</sub>, corresponding to  $\sim 10-20 \text{ mmol L}^{-1} \text{ Na}_{2}\text{Cr}_{2}\text{O}_{7}$ .

Figure 6 shows that molybdate does not significantly affect the HER Faradaic efficiency on platinum in the NaClO-containing electrolyte. There is a small enhancement in the efficiency when 80 mmol  $L^{-1}$  molybdate is in the electrolyte, as shown by the blue bars in Fig. 6. However,  $> 40 \text{ mmol L}^{-1}$  molybdate in solution has been shown to enhance O<sub>2</sub> formation, <sup>17</sup> detrimentally affecting the anode efficiency and raising safety concerns (due to the risk of reaching an explosive mixture in the hydrogen-containing cell gas). These results allow us to unravel the oxygen formation and to evaluate the effect of molybdate on it.

The volumetric flow of oxygen generated during galvanostatic electrolysis as a function of the additives (Supporting Information Fig. S8) shows a sudden fast increase of the oxygen signal at the beginning of the experiment (t < 5 min) and a monotonic signal decrease after  $\sim$ 5 min. The behavior at about t < 5 min has been previously observed for the chemical decomposition of hypochlorite. 15,52 There are several possible sources of oxygen in the chlorate electrolysis cell: coming from (i) anodic reactions so called electrochemically produced oxygen, or (ii) chemical heterogeneous decomposition of hypochlorite forming oxygen where the electrode surface catalyzes the oxygen formation, and

10974660, 2023, 5, Downloaded from https://onlinelibrary.wiely.com/doi/10.1002/jctb.7345 by Cochrane Netherlands, Wiley Online Library on [1809/2023]. See the Terms and Conditions (https://onlinelibrary.wiely.com/rems-and-conditions) on Wiley Online Library for rules of use; OA articles are governed by the applicable Creative Commons Licenson





**Figure 6.** Effect of electrolyte additives on the Faradaic efficiency towards HER on a Pt foil, measured in NaCl 2 moll<sup>-1</sup> with NaClO at an initial concentration of 80 mmol L<sup>-1</sup> (depicted in the plot as no additives). Measurements were made a pH 6.5 and 80 °C during a galvanostatic electrolysis at 300 mA cm<sup>-2</sup> (electrode geometrical area: 0.5 cm<sup>2</sup>).

(iii) from homogeneous hypochlorite decomposition in the bulk.  $^{32}$  The MS results (Supporting Information Fig. S8) further show that the concentration of  $Na_2Cr_2O_7$  does not significantly affect either the chemical decomposition of hypochlorite (i.e. no significant differences in the oxygen maximum at the beginning of the experiment) or the electrochemical oxygen production (depicted as a sharp decrease in the  $O_2$  signal upon turning the current off). On the contrary, 80 mmol  $L^{-1}$  of molybdate both promotes the chemical decomposition of NaClO (see Fig. 7) and enhances the electrochemically produced oxygen, seen as the drop in Supporting Information Fig. S7 once the current was switched off. Still, our MS results show that 10 mmol  $L^{-1}$  molybdate in the electrolyte does not promote the formation of oxygen compared to the measurement without additives.

These results are in line with previous reports from our group, concluding that molybdate at low concentration (10 mmol L<sup>-1</sup>) does not significantly affect the chemical decomposition of hypochlorite into oxygen.<sup>52</sup> Given the presented experimental data, chemical decomposition is avoided at a concentration of 10 mmol L<sup>-1</sup> molybdate (Fig. 7 and Supporting Information Fig. S9). Following

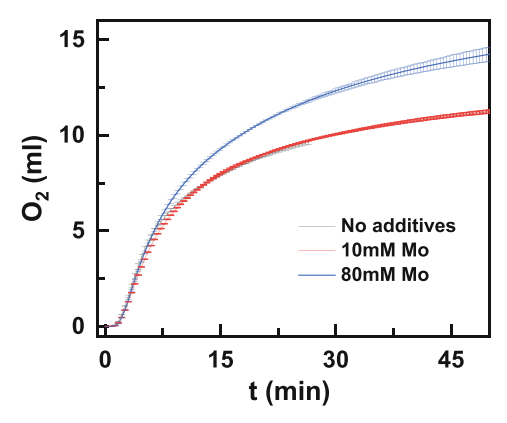


**Figure 7.** Volume of oxygen produced by homogeneous decomposition of hypochlorite in 2 mol  $L^{-1}$  NaCl, 80 mmol  $L^{-1}$  NaClO (initially), pH 6.5 and 80 °C, with and without molybdenum addition.

hypochlorite concentration (Supporting Information Table S1) indicated that addition of 10 mmol  $L^{-1}$  molybdate does not significantly affect the rate constant for the hypochlorite decomposition compared to the case without additives. However, in the case of 80 mmol  $L^{-1}$  molybdate the rate constant for the hypochlorite decomposition was increased by  $\sim 30\%$ .

Both the overpotential for HER and the rate of unwanted oxygen evolution increase at high concentrations of molybdate, while the hydrogen Faradaic efficiency does not depend much on the concentration of molybdate (range 10–80 mmol  $L^{-1}$ ). We show that by fine-tuning the molybdate concentration in the range 10–30 mmol  $L^{-1}$  a high Faradaic efficiency and activity towards the HER can be obtained without promoting  $\rm O_2$  generation.

Coatings of Cr and Mo may be formed *in situ* or *ex situ*. The former has the advantage of a continuously refreshed electrode surface, where cracks etc. in the coating are mended during operation, as is the case with the chromate addition today. The latter allows a better control of the composition and morphology of the protective layer, and has shown promising results.<sup>20</sup> We show that Mo is important for the stability of the selective Cr layer.

#### **CONCLUSIONS**

This work has quantitatively addressed the effect of additives, namely  $Na_2Cr_2O_7$  (in the micromolar range) and  $Na_2MoO_4$  (in the millimolar range), on the production of  $H_2$  and  $O_2$  from NaClO-containing electrolytes using inert Pt as cathode material. Films formed from these additives were examined by SEM and EDX, where only the platinum surface could be recorded, as most likely the deposited films were of nanometer thickness. XPS studies of the as-deposited films revealed a partial reduction in Mo oxidation states compared to the electrolytic solution. Their oxidation states and oxidation state percentages were highly dependent on the deposition conditions (concentration of additives and temperature). In the presence of Cr it is likely that only trace levels of Mo are deposited as XPS could not detect any traces of Mo in such films.

10974660, 2023, 5, Downloaded from https://onlinelibrary.wiley.com/doi/10.1002/jctb.7345 by Cochrane Netherlands, Wiley Online Library on [18/09/2023]. See the Terms and Conditions (https://onlinelibrary.wiley.com/terms-and-conditions) on Wiley Online Library for rules of use; OA articles are governed by the

Still molybdate, particularly at electrolyte concentrations of 10 mmol L<sup>-1</sup> Mo, has a strong activating effect towards HER on Pt and additionally enhances the stability of the chromium hydroxide film at open circuit. The electrocatalytic effect is also preserved when Cr and Mo are combined, leading to a shift of 260 mV to less negative potentials at current densities of 300 mA cm<sup>-2</sup> compared to measurements in molybdate-free electrolytes.

The Faradaic efficiency towards hydrogen evolution can be enhanced by more than 15% in the presence of 3  $\mu$ mol L<sup>-1</sup> Na<sub>2</sub>Cr<sub>2</sub>O<sub>7</sub>. Na<sub>2</sub>MoO<sub>4</sub> as a co-additive has a minor effect on the hydrogen Faradaic efficiency at a high concentration (80 mmol L<sup>-1</sup>). However, such high concentration enhances the chemical and electrochemical reactions leading to O<sub>2</sub>, which is detrimental for the chlorate process, whereas 10 mmol L<sup>-1</sup> Mo does not affect homogeneous hypochlorite decomposition or oxygen generation in the cell.

Our finding allows us to optimize molybdate concentration further to obtain the highest hydrogen evolution efficiency and film stability while minimizing O2 generation even at micromolar chromate levels. The insights on the synergy of Cr-Mo could also be capitalized for photocatalytic hydrogen production and the degradation of industrial wastewater. However, the influence of the investigated additives on the reduction of chlorate ions still remains to be investigated. Also, as it is unclear how the films combining Cr and Mo are formed, more investigations to enlighten this synergy are needed. Related to this is how to produce such films in an industrial process – in situ or ex situ. The findings presented in this paper may be applicable to the next generation of sodium chlorate process technology where a more active and stable cathode material is used which also requires a much higher electrolyte purity compared to the industrial standard today 47,53-55 To further elucidate the commercial viability of these results, further research should focus on applying more industrial conditions by, for instance, using electrolytes containing high ionic strength and disturbing agents such as calcium or sulfates.

#### **ACKNOWLEDGEMENTS**

The assistance of Björn Eriksson with SEM imaging is appreciated. Financial support from the Swedish Energy Agency (project 40535-1) and Nouryon AB is gratefully acknowledged. We would also like to acknowledge the central lab facility at Ångstromlaboratriet, MY Fab lab, and the funding agency Knut and Alice Wallenberg Foundation for the XPS instrument. These authors contributed equally: Oscar Diaz-Morales and Aleksandra Lindberg.

#### SUPPORTING INFORMATION

Supporting information may be found in the online version of this article.

## **REFERENCES**

- 1 Held, H.; Gao, A.; Funada, C.; Schlag, S.; Beraud, L. IHS Chemical Economics Handbook; S&P Global Commodity Insights, 2021.
- 2 Suhr M, Klein G, Kourti I, Rodrigo Gonzalo M, Giner Santonja G, Roudier S and Delgado Sancho L, Best Available Techniques (BAT) Reference Document for the Production of Pulp, Paper and Board. Industrial Emissions Directive 2010/75/EU, Seville, Spain, 2015.
- 3 Cornell A, Chlorate synthesis cells and technology, in *Encyclopedia of Applied Electrochemistry*, ed. by Kreysa G, Ota K and Savinell RF. Springer New York, New York, NY, pp. 181–187 (2014).

- 4 Endrődi B, Simic N, Wildlock M and Cornell A, A review of chromium(VI) use in chlorate electrolysis: functions, challenges and suggested alternatives. *Electrochim Acta* 234:108–122 (2017 Apr).
- 5 Karlsson RKB and Cornell A, Selectivity between oxygen and chlorine evolution in the Chlor-alkali and chlorate processes. Chem Rev 116: 2982–3028 (2016).
- 6 Gomes ASO, Busch M, Wildlock M and Simic N, Understanding selectivity in the chlorate process: a step towards efficient hydrogen production. Chemistry Select 3:6683–6690 (2018).
- 7 Kimbrough DE, Cohen Y, Winer AM, Creelman L and Mabuni C, A critical assessment of chromium in the environment. *Crit Rev Environ Sci Technol* **29**:1–46 (1999).
- 8 McNeill L, McLean J, Edwards M and Parks J, State of the science of hexavalent chromium in drinking water. Water Res Found 6666: 1–35 (2012).
- 9 Mishra S and Bharagava RN, Toxic and genotoxic effects of hexavalent chromium in environment and its bioremediation strategies. *J Environ Sci Heal - Part C Environ Carcinog Ecotoxicol Rev* **34**:1–32 (2016).
- 10 Herlitz F, Inhibiting effect of oxidized zirconium on parasitic cathodic reactions in the sodium chlorate process. Part I: hypochlorite reduction. J Appl Electrochem 31:307–311 (2001).
- 11 Gustavsson J, Li G, Hummelgard C, Backstrom J and Cornell A, On the suppression of cathodic hypochlorite reduction by electrolyte additions of molybdate and chromate ions. *J Electrochem Sci Eng* 2:185– 198 (2012).
- 12 Hedenstedt K, Gomes ASO, Busch M and Ahlberg E, Study of hypochlorite reduction related to the sodium chlorate process. *Electrocatalysis* 7:326–335 (2016).
- 13 Endrődi B, Sandin S, Smulders V, Simic N, Wildlock M, Mul G, Mei B and Cornell A, Towards sustainable chlorate production: the effect of permanganate addition on current efficiency. J Clean Prod 182: 529–537 (2018).
- 14 Endrődi B, Smulders V, Simic N, Wildlock M, Mul G, Mei B and Cornell A, In situ formed vanadium-oxide cathode coatings for selective hydrogen production. *Appl Catal Environ* **244**(September 2018):233–239 (2019).
- 15 Endrődi B, Sandin S, Wildlock M, Simic N and Cornell A, Suppressed oxygen evolution during chlorate formation from hypochlorite in the presence of chromium(VI). J Chem Technol Biotechnol 94:1520– 1527 (2019).
- 16 Endrődi B, Diaz-Morales O, Mattinen U, Cuartero M, Padinjarethil AK, Simic N, Wildlock M, Crespo G and Cornell A, Selective electrochemical hydrogen evolution on cerium oxide protected catalyst surfaces. *Electrochim Acta* 341:136022 (2020).
- 17 Li M, Twardowski Z, Mok F and Tam N, Sodium molybdate-a possible alternate additive for sodium dichromate in the electrolytic production of sodium chlorate. J Appl Electrochem 37:499–504 (2007).
- 18 Smulders V, Gomes ASO, Simic N, Mei B and Mul G, Mixed chromate and molybdate additives for cathodic enhancement in the chlorate process. *Electrocatalysis* 12:447–455 (2021).
- 19 Gustavsson J, Hummelgard C, Backstrom J, Wallinder IO, Rahman SM, Lindbergh G, Erikssson S and Cornell A, In-situ activated hydrogen evolution by molybdate addition to neutral and alkaline electrolytes. J Electrochem Sci Eng. 2:105–120 (2012).
- 20 Lačnjevac UC, Jović BM, Gajić-Krstajić LM, Kovač J, Jović VD and Krstajić NV, Ti substrate coated with composite Cr-MoO<sub>2</sub> coatings as highly selective cathode materials in hypochlorite production. *Electrochim Acta* 96:34–42 (2013).
- 21 Hedenstedt K, Bäckström J and Ahlberg E, In-situ Raman spectroscopy of  $\alpha$  and  $\gamma$ -FeOOH during cathodic load. *J Electrochem Soc* **164**: H621–H627 (2017).
- 22 Vogt H, Balej J, Bennett JE, Wintzer P, Sheikh SA and Gallone PVSPK, Chlorine Oxides and Chlorine Oxygen Acids in "Ullmann's Encyclopedia of Industrial Chemistry.". Wiley-VCH Verlag GmbH & Co. KGaA, Weinheim, Germany pp. 624–680 (2010).
- 23 McCrum IT and Koper MTM, The role of adsorbed hydroxide in hydrogen evolution reaction kinetics on modified platinum. *Nat Energy* 5: 891–899 (2020).
- 24 Yu X, dos Santos EC, White J, Salazar-Alvarez G, Pettersson LGM, Cornell A and Johnsson M, Electrocatalytic glycerol oxidation with concurrent hydrogen evolution utilizing an efficient MoO x /Pt catalyst. **17**:2104288 (2021).
- 25 Busser GW, Mei B, Weide P, Vesborg PCK, Stührenberg K, Bauer M, Huang X, Willinger M-C, Chorkendorff I and Schlögl R, Muhler M,

10974660, 2023, 5, Downloaded from https://onlinelibrary.wiely.com/doi/10.1002/jctb.7345 by Cochrane Netherlands, Wiley Online Library on [1809/2023]. See the Terms and Conditions (https://onlinelibrary.wiely.com/rems-and-conditions) on Wiley Online Library for rules of use; OA articles are governed by the applicable Creative Commons Licenson

- Cocatalyst designing: a regenerable molybdenum-containing ternary cocatalyst system for efficient photocatalytic water splitting. ACS Catal **5**:5530–5539 (2015).
- 26 Chiang TH, Lyu H, Hisatomi T, Goto Y, Takata T, Katayama M, Minegishi T and Domen K, Efficient photocatalytic water splitting using Al-doped SrTiO3Coloaded with molybdenum oxide and rhodium-chromium oxide. ACS Catal. 8:2782–2788 (2018).
- 27 Goto Y, Hisatomi T, Wang Q, Higashi T, Ishikiriyama K, Maeda T, Sakata Y, Okunaka S, Tokudome H, Katayama M, Akiyama S, Nishiyama H, Inoue Y, Takewaki T, Setoyama T, Minegishi T, Takata T, Yamada T and Domen K, A particulate photocatalyst water-splitting panel for large-scale solar hydrogen generation. *Joule* 2:509–520 (2018 Mar).
- 28 Qureshi M, Shinagawa T, Tsiapis N and Takanabe K, Exclusive hydrogen generation by electrocatalysts coated with an amorphous chromium-based layer achieving efficient overall water splitting. *ACS Sustain Chem Eng.* **5**:8079–8088 (2017).
- 29 Obata K, Shinohara Y, Tanabe S, Waki I, Kotsovos K, Ohkawa K and Takanabe K, A stand-alone module for solar-driven H<sub>2</sub> production coupled with redox-mediated sulfide remediation. *Energ Technol* **7**: 1–13 (2019).
- 30 Yoshida M, Takanabe K, Maeda K, Ishikawa A, Kubota J, Sakata Y, Ikezawa Y and Domen K, Role and function of Noble-metal/Cr-layer Core/Shell structure cocatalysts for photocatalytic overall water splitting studied by model electrodes. *J Phys Chem C* **113**:10151–10157 (2009).
- 31 Copyright © 2005 Casa Software Ltd.
- 32 Lindberg A, Diaz-Morales O, Holmin S and Cornell A, Sources of oxygen produced in the chlorate process utilizing dimensionally stable anode (DSA) electrodes doped by Sn and Sb. *Ind Eng Chem Res.* **60**:13505–13514 (2021).
- 33 Cornell A, Håkansson B and Lindbergh G, Ruthenium-based dimensionally stable anode in chlorate electrolysis. J Electrochem Soc 150:D6 (2003).
- 34 Endrődi B, Stojanovic A, Cuartero M, Simic N, Wildlock M, de Marco R, Crespo G and Cornell A, Selective hydrogen evolution on manganese oxide coated electrodes: new cathodes for sodium chlorate production. ACS Sustain Chem Eng 7:1–8 (2019).
- 35 Et AT, X-Ray-Data-Booklet Rev 3. Lawrence Berkeley National Laboratory, Berkeley, CA (2009).
- 36 Ramana CV and Julien CM, Chemical and electrochemical properties of molybdenum oxide thin films prepared by reactive pulsed-laser assisted deposition. Chem Phys Lett 428:114–118 (2006).
- 37 Ramana CV, Atuchin VV, Pokrovsky LD, Becker U and Julien CM, Structure and chemical properties of molybdenum oxide thin films. J Vac Sci Technol A 25:1166–1171 (2007).
- 38 Spevack PA and McIntyre NS, A Raman and XPS investigation of supported molybdenum oxide thin films. 2. Reactions with hydrogen sulfide. J Phys Chem 97:11031–11036 (1993).

- 39 Choi J-G and Thompson LT, XPS study of as-prepared and reduced molybdenum oxides. Appl Surf Sci 93:143–149 (1996).
- 40 Baltrusaitis J, Mendoza-Sanchez B, Fernandez V, Veenstra R, Dukstiene N, Roberts A and Fairley N, Generalized molybdenum oxide surface chemical state XPS determination via informed amorphous sample model. *Appl Surf Sci* 326:151–161 (2015).
- 41 Conway BE and Bai L, Determination of adsorption of OPD H species in the cathodic hydrogen evolution reaction at Pt in relation to electrocatalysis. J Electroanal Chem Interfacial Electrochem 198:149–175 (1986).
- 42 Subbaraman R, Tripkovic D, Strmcnik D, Chang KC, Uchimura M, Paulikas AP, Stamenkovic V and Markovic N, Enhancing hydrogen evolution activity in water splitting by tailoring Li<sup>+</sup>-Ni(OH)<sub>2</sub>-Pt interfaces. *Science* **334**:1256–1260 (2011).
- 43 Li J, Li B, Huang H, Yan S, Yuan C, Wu N and Guo D, Liu X, Polyvinylpyr-rolidone gel based Pt/Ni(OH)<sub>2</sub> heterostructures with redistributing charges for enhanced alkaline hydrogen evolution reaction. J Mater Chem A 9:27061–27071 (2021).
- 44 Zhang C, Liang X, Xu R, Dai C, Wu B, Yu G, Chen B, Wang X and Liu N, H<sub>2</sub> In situ inducing strategy on Pt surface segregation over low Pt doped PtNi<sub>5</sub> nanoalloy with superhigh alkaline HER activity. *Adv Funct Mater* **31**:1−11 (2021).
- 45 Shinagawa T, Garcia-Esparza AT and Takanabe K, Insight on Tafel slopes from a microkinetic analysis of aqueous electrocatalysis for energy conversion. *Sci Rep* **5**:13801 (2015).
- 46 Wulff J and Cornell A, Cathodic current efficiency in the chlorate process. J Appl Electrochem 37:181–186 (2006).
- 47 Rosvall M., Hedenstedt K., Sellin A., Gustavsson J. and Cornell A.. Activation of cathode, US Patent US009689077B2. 2017.
- 48 Lindbergh G and Simonsson D, The effect of chromate addition on cathodic reduction of hypochlorite in hydroxide and chlorate solutions. *J Electrochem Soc* **137**:3094–3099 (1990).
- 49 Lindbergh G and Simonsson D, Inhibition of cathode reactions in sodium hydroxide solution containing chromate. *Electrochim Acta* **36**:1985–1994 (1991).
- 50 Gomes ASO, Simic N, Wildlock M, Martinelli A and Ahlberg E, *Electrochemical investigation of the hydrogen evolution reaction on electrodeposited films of Cr(OH)*<sub>3</sub> *and Cr*<sub>2</sub>O<sub>3</sub> *in mild alkaline solutions. Electrocatalysis* **9**:333–342 (2018).
- 51 Smulders V, Simic N, Gomes ASO, Mei B and Mul G, Electrochemical formation of Cr(III)-based films on Au electrodes. *Electrochim Acta* **296**: 1115–1121 (2019).
- 52 Sandin S, Karlsson RKB and Cornell A, Catalyzed and uncatalyzed decomposition of hypochlorite in dilute solutions. *Ind Eng Chem Res* **54**:3767–3774 (2015).
- 53 Rosvall M, Amerio E, Gustavsson J, Holmin S B LE. Electrode. US Patent; 11326266. 2022.
- 54 Rosvall M and Nordin B. Electrode. US Patent; 11041249, 2021.
- 55 Rosvall M, Edvinsson-Albers R HK. Electrode US Patent; 8764963, 2014.